

Article

# A Porphyrinic Zirconium Metal-Organic Framework for Oxygen Reduction Reaction: Tailoring the Spacing between Active-Sites through Chain-Based Inorganic Building Units

Magdalena Ola Cichocka, Zuozhong Liang, Dawei Feng, Seoin Back, Samira Siahrostami, Xia Wang, Laura Samperisi, Yujia Sun, Hongyi Xu, Niklas Hedin, Haoquan Zheng, Xiaodong Zou, Hong-Cai Zhou, and Zhehao Huang

*J. Am. Chem. Soc.*, **Just Accepted Manuscript** • DOI: 10.1021/jacs.0c06329 • Publication Date (Web): 10 Aug 2020

Downloaded from pubs.acs.org on August 10, 2020

## Just Accepted

"Just Accepted" manuscripts have been peer-reviewed and accepted for publication. They are posted online prior to technical editing, formatting for publication and author proofing. The American Chemical Society provides "Just Accepted" as a service to the research community to expedite the dissemination of scientific material as soon as possible after acceptance. "Just Accepted" manuscripts appear in full in PDF format accompanied by an HTML abstract. "Just Accepted" manuscripts have been fully peer reviewed, but should not be considered the official version of record. They are citable by the Digital Object Identifier (DOI®). "Just Accepted" is an optional service offered to authors. Therefore, the "Just Accepted" Web site may not include all articles that will be published in the journal. After a manuscript is technically edited and formatted, it will be removed from the "Just Accepted" Web site and published as an ASAP article. Note that technical editing may introduce minor changes to the manuscript text and/or graphics which could affect content, and all legal disclaimers and ethical guidelines that apply to the journal pertain. ACS cannot be held responsible for errors or consequences arising from the use of information contained in these "Just Accepted" manuscripts.

# A Porphyrinic Zirconium Metal-Organic Framework for Oxygen Reduction Reaction: Tailoring the Spacing between Active-Sites through Chain-based Inorganic Building Units

Magdalena Ola Cichocka,<sup>‡,†</sup> Zuozhong Liang,<sup>#,†</sup> Dawei Feng,<sup>§</sup> Seoin Back,<sup>°</sup> Samira Siahrostami,<sup>‡</sup> Xia Wang,<sup>‡</sup> Laura Samperisi,<sup>‡</sup> Yujia Sun,<sup>§</sup> Hongyi Xu,<sup>‡</sup> Niklas Hedin,<sup>‡</sup> Haoquan Zheng,<sup>\*,#</sup> Xiaodong Zou,<sup>‡</sup> Hong-Cai Zhou<sup>\*,§,||</sup> and Zhehao Huang<sup>\*,‡</sup>

<sup>‡</sup>Department of Materials and Environmental Chemistry, Stockholm University, Stockholm SE-106 91, Sweden

<sup>§</sup>Department of Chemistry, Texas A&M University, College Station, Texas 77843-3255, United States

<sup>#</sup>Key Laboratory of Applied Surface and Colloid Chemistry, Ministry of Education, School of Chemistry and Chemical Engineering, Shaanxi Normal University, Xi'an 710119, China.

<sup>°</sup>Department of Chemical and Biomolecular Engineering, Sogang University, Seoul 04107, Republic of Korea

<sup>‡</sup>Department of Chemistry, University of Calgary, 2500 University Drive NW, Calgary, Alberta T2N1N4, Canada

<sup>||</sup>Department of Materials Science and Engineering, Texas A&M University, College Station, Texas 77843-3003, United States

## ABSTRACT:

The oxygen reduction reaction (ORR) is central in carbon-neutral energy devices. While platinum group materials have shown high activities for ORR, their practical uses are hampered by concerns over deactivation, slow kinetics, exorbitant cost, and scarce nature reserve. The low-cost yet high tunability of metal-organic frameworks (MOFs) provide a unique platform for tailoring their characteristic properties as new electrocatalysts. Herein, we report a new concept of design and present stable Zr-chain-based MOFs as efficient electrocatalysts for ORR. The strategy is based on using Zr-chains to promote high chemical and redox stability, and more importantly, tailor the immobilization and packing of redox active-sites at an ideal density to improve the reaction kinetics. The obtained new electrocatalyst, PCN-226, thereby shows high ORR activity. We further demonstrate PCN-226 as a promising electrode material for practical applications in rechargeable Zn-air batteries, with a high peak power density of 133 mW cm<sup>-2</sup>. Being one of the very few electrocatalytic MOFs for ORR, this work provides a new concept by designing chain-based structures to enrich the diversity of efficient electrocatalysts and MOFs.

## INTRODUCTION

The increasing global demands for sustainable energy simultaneously drive the development of new devices for energy conversion. Oxygen reduction reaction (ORR) plays a crucial role in such type of devices including fuel cells and metal-air batteries.<sup>1,2</sup> Platinum group materials are the predominate class of materials that are used as electrocatalysts for ORR.<sup>3</sup> However, their scarcity, high cost, low

1 reaction kinetics, and stability prevent their widespread implementation in commercial green energy  
2 applications. Thus, driven by the crucial importance of the ORR in energy conversion processes,  
3 numerous systems based on non-precious elements have been developed in the search for low-cost and  
4 stable candidates with good electrocatalytic activities.<sup>4–8</sup> In addition, high surface area scaffolds are  
5 paramount in the development of electrocatalysts for their implementations in various practical devices  
6 concerning deactivation, recyclability, and water solubility.

7  
8  
9 Metal-organic frameworks (MOFs) are porous inorganic-organic hybrid materials with extraordinary  
10 high surface areas<sup>9,10</sup> With high accessibility to the active-sites, MOFs take the dual roles acting as both  
11 catalysts and porous supports in heterogeneous catalysis. Notably, immobilizing catalytic sites in the  
12 well-defined structures, it can effectively limit deactivation pathways.<sup>11,12</sup> An important advantage of  
13 MOFs compared to carbon and metal oxides based materials is the possibility to easily and  
14 systematically design and alter the pores size and functionality at a molecular level by applying reticular  
15 chemistry.<sup>13</sup> Compared to noble metals, which are mostly non-porous, the fast mass transport inside  
16 crystals, as well as their low cost endow MOFs as a promising class of materials in the energy storage  
17 and conversion field.<sup>14–20</sup> To further tackle their charge transport ability, MOFs have been designed  
18 either by orbital overlapping and charge delocalization between linkers,<sup>21–26</sup> or by introducing redox-  
19 active molecular linkers<sup>27–29</sup>. Metalloporphyrin complexes exhibit strong interactions with O<sub>2</sub>, and offer  
20 a good opportunity by serving as a channel for electron transfer via a hopping mechanism.<sup>30–32</sup>  
21 Moreover, the rich chemistry and the high electrochemical stability of metalloporphyrin complexes  
22 endow porphyrinic MOFs as designable and durable electrocatalysts. Recently, such MOFs have been  
23 successfully utilized for the electrocatalytic hydrogen evolution reaction (HER),<sup>33,34</sup> CO<sub>2</sub> reduction  
24 reaction (CO<sub>2</sub>RR),<sup>35–37</sup> oxygen evolution reaction (OER),<sup>38–40</sup> and oxygen reduction reaction (ORR),<sup>41–</sup>  
25 44 etc. By efficiently limiting the deactivation pathways related to the electrocatalytic sites, these MOFs  
26 show electrochemical activities and relatively stable cycling. However, the structural and chemical  
27 stabilities of MOFs, and more importantly, the sparse active-sites in most studied MOFs are the major  
28 drawbacks, which have rendered such MOFs with limited redox capabilities.

29  
30  
31 Herein, we report the design of a new MOF, denoted PCN-226, which is built by linking redox active  
32 metalloporphyrins and Zr(+4) cations. Because of using earth abundant elements, it significantly  
33 reduces the producing cost compared to noble metal-based materials. Moreover, according to the Hard  
34 Soft Acid Base (HSAB) theory, Zr(+4) cations have strong affinity with carboxyl-functionalized  
35 metalloporphyrins, and are able to produce stable MOFs.<sup>45</sup> In addition to the stable, accessible and  
36 redox active-sites for ORR, the MOF was designed uniquely based on an infinitive zigzag Zr-oxide  
37 chain structure. The chain-based structure not only enhances the overall stability of the MOF but also  
38 allows the redox active-sites at a close space to give rise to high reaction kinetics and catalyst loadings.  
39 The density of catalytically active-sites of PCN-226 is the highest among the reported porphyrinic Zr-  
40 MOFs. We prepared PCN-226 nanocrystals to improve the diffusion kinetics of adsorbed and reacting  
41 molecules. The structure of PCN-226 was determined by continuous rotation electron diffraction  
42 (cRED)<sup>46,47</sup> or microcrystal electron diffraction (MicroED)<sup>48</sup>. As an electrocatalyst for ORR, PCN-226  
43 showed high activity and reaction kinetics, especially compared to cluster-based MOFs. When applied  
44 as electrodes for practical application in a rechargeable Zn-air battery, PCN-226 exhibited a high peak  
45 power density of 133 mW cm<sup>-2</sup>. The integrity of PCN-226 remained intact after ORR.

## RESULTS AND DISCUSSION

**Synthesis and Characterization.** The Zr-chain building units have firstly been reported in the MIL-140 series.<sup>49</sup> Owing to the high connectivity of Zr and robustness of the oxide chain unit, these structures show high mechanical, thermal, and hydrothermal stability compared to the UiO series Zr-MOFs based on the Zr<sub>6</sub>-oxo cluster.<sup>49</sup> Yet, such Zr-oxide chain structure has been found so far only in MIL-140 and MIL-163 and their derivatives,<sup>49,50</sup> presumably due to the lack of rationale for synthesis of such building unit. In particular, in the reported porphyrinic Zr-MOFs, the Zr<sub>6</sub>-oxo cluster (ZrO<sub>4</sub>(OH)<sub>4</sub>) is dominating and adopts versatile connecting modes and yields different structures with outstanding stabilities.<sup>51–58</sup> Due to the large size of the porphyrinic linker, the metalloporphyrin centers in these structures are isolated by the Zr<sub>6</sub>-oxo nodes, preventing collaborative catalytic processes in the frameworks. To avoid the formation of the Zr<sub>6</sub>-oxo phases, we herein adopt a thermodynamically controlled synthesis to enforce the formation of the Zr-oxide chain structure. Specifically, we conducted the reaction at a higher temperature (140 °C) than that in a typical Zr-MOF synthesis and added a high excess of benzoic acid (BA, BA/Zr = 67, molar ratio) as a competing reagent. As the BA can competitively coordinate to Zr atoms to control both the kinetics and thermodynamics of the Zr-MOF formation (Scheme S2), a large amount of BA can inhibit the formation of Zr<sub>6</sub>-oxo containing structures with lower thermodynamic stability. Meanwhile, higher reaction temperatures can facilitate the formation of Zr chains by overcoming the associated higher energetic barrier, as compared to the formation of kinetically favored Zr<sub>6</sub> clusters in typical Zr-MOFs. As expected, we obtained a Zr-oxide chain-based framework PCN-226. By applying the same strategy, isostructural MOFs with uncoordinated porphyrin and different metalloporphyrins, containing ions of metals such as Cu, Co, Ni, Fe, and Zn, have been successfully obtained, creating a new series of ultra-stable porphyrinic Zr-MOFs.

The resulting MOF, PCN-226(Cu), was characterized by powder X-ray diffraction (PXRD), which shows the high crystallinity of the MOF with intense and sharp peaks (Figure 1a). Moreover, the features in the PXRD patterns (Figure S1) show that a series of isostructural PCN-226s could be synthesized with the same structure and topology. Scanning electron microscopy (SEM) images show a plank-like crystal morphology of the MOF with 1–20 μm in length and ca. 500 nm in thickness (Figure S2). Continuous rotation electron diffraction (cRED) was applied for *ab initio* structure determination of PCN-226(Cu) and PCN-226(Co), respectively. The unit cell parameters obtained from the cRED data were refined against PXRD data by using the Pawley method, and the structural models were refined against cRED data (Figures 1b–g, S3, S4, and Table S1–3, see Supporting Information for more details). The refinement results further confirm that PCN-226s have the same structure. As expected from our synthetic strategy, the three-dimensional (3D) structure is constructed by linking infinite zigzag ZrO<sub>7</sub> chains with metalloporphyrin molecules (Figure 2). Interestingly, besides the carboxylates from metalloporphyrin, BAs also connected to the Zr-oxo chains (Figure S5). This connection indicates the importance of using excessive BAs in the synthesis, where BAs inhibit the formation of Zr<sub>6</sub>-oxo clusters and favor the formation of Zr-oxide chains by coordinating to the Zr(+4) cations. To the best of our knowledge, the unique chain structure endows PCN-226 with a novel topology that has never been reported. The metal loadings in the porphyrins of PCN-226(Cu) and PCN-226(Co) were 79.4%, and 87.2%, respectively, which was calculated from inductively coupled plasma optical emission spectroscopy (ICP-OES) (Table S4).

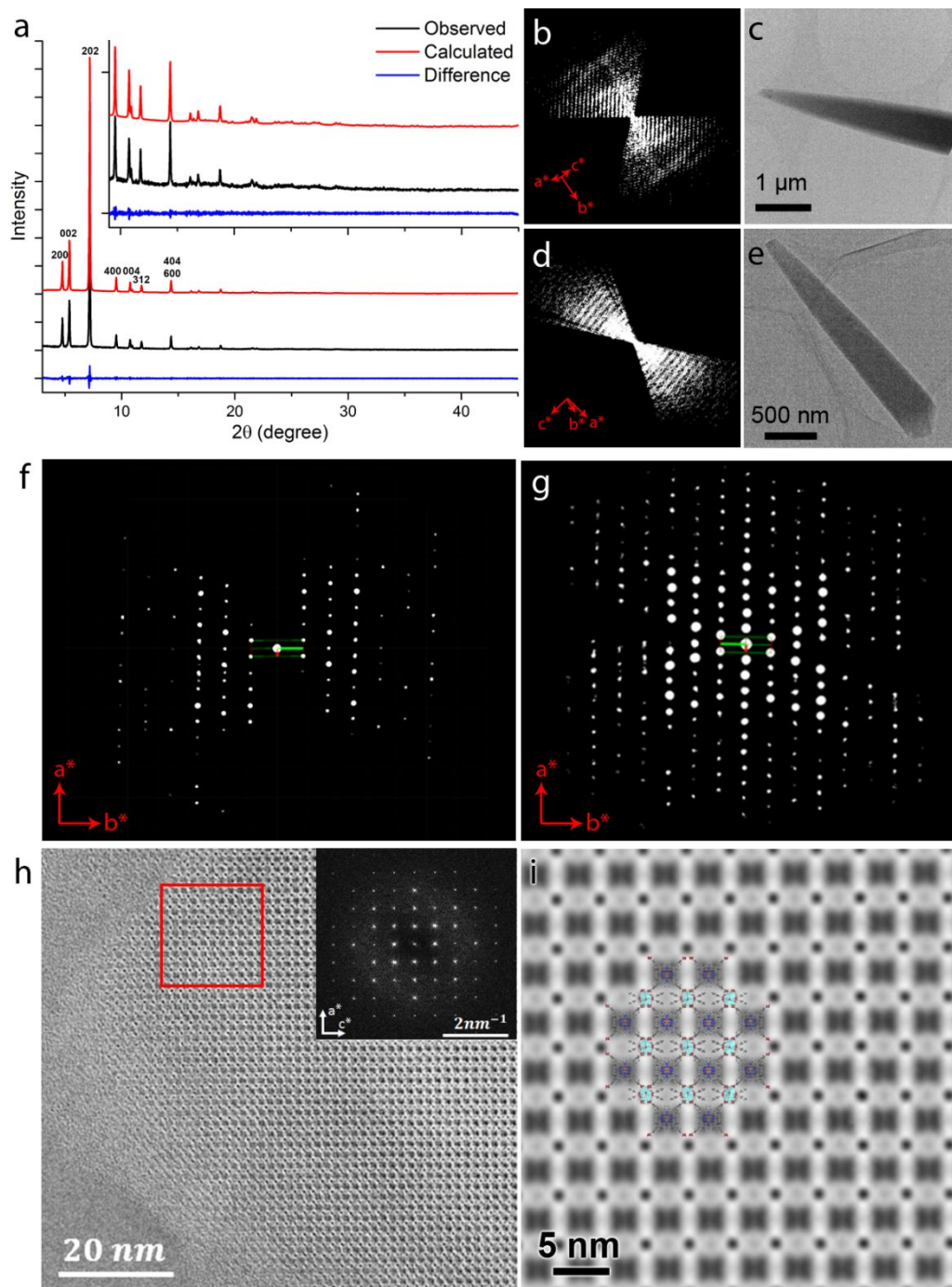


**Figure 1.** (a) Pawley fit of the experimental PXRD pattern ( $\lambda = 1.5406 \text{ \AA}$ ) of PCN-226, showing a good agreement. (b and d) Reconstructed 3D reciprocal lattice of PCN-226(Cu) and PCN-226(Co), respectively. (c and e) The particles from which the cRED data was collected. (f and g) The  $hk0$  reciprocal planes of PCN-226(Cu) and PCN-226(Co), respectively, showing a similar intensity distribution. (h) HRTEM image of PCN-226(Cu) along the  $[010]$  direction that shows a rectangular pore packing with  $d_{200} = 18.32 \text{ \AA}$  and  $d_{002} = 16.18 \text{ \AA}$  (calculated  $d_{200} = 18.53 \text{ \AA}$  and  $d_{002} = 16.25 \text{ \AA}$ ). Inset: Fourier transform of the image. (i) Symmetry imposed HRTEM image from the region highlighted by the red square in h). The structural model of PCN-226(Cu) is superimposed in the image showing the good agreement.

PCN-226 contains two topologically distinct yet interconnected channels along the  $[010]$  and  $[001]$  directions, respectively (Figures 2c, 2d and S6). The chain-based structure effectively limits the spacing and results in a high packing density of metalloporphyrins, where the electrochemical active-sites are



loaded. Based on the crystal structures, the packing density of PCN-226 is 1.4 – 11.0 times higher compared to other reported porphyrinic Zr-MOFs (Table 1). HRTEM images clearly show the rectangular pore arrangement (Figures 1h and i), which is in good agreement with the structural model. The permanent porosity of PCN-226 was further estimated by analysis of the N<sub>2</sub> sorption isotherm at 77 K. A N<sub>2</sub> uptake of 10.1 mmol g<sup>-1</sup> and a Brunauer-Emmett-Teller (BET) surface area of 800 m<sup>2</sup> g<sup>-1</sup> were calculated for PCN-226(Cu) (Figure S7). The experimental surface area was slightly larger than the theoretical value of PCN-226(Cu) of 621 m<sup>2</sup> g<sup>-1</sup> based on the structural model, indicating the formation of possible defects with missing linkers. Simulation from the N<sub>2</sub> adsorption isotherm based on non-local density functional theory (NLDT) gave a pore size distribution in the range of 5.3 – 7.8 Å. Other PCN-226 MOFs with different metalloporphyrins show similar N<sub>2</sub> uptake, surface area, and pore size distribution (Figures S8-S12).

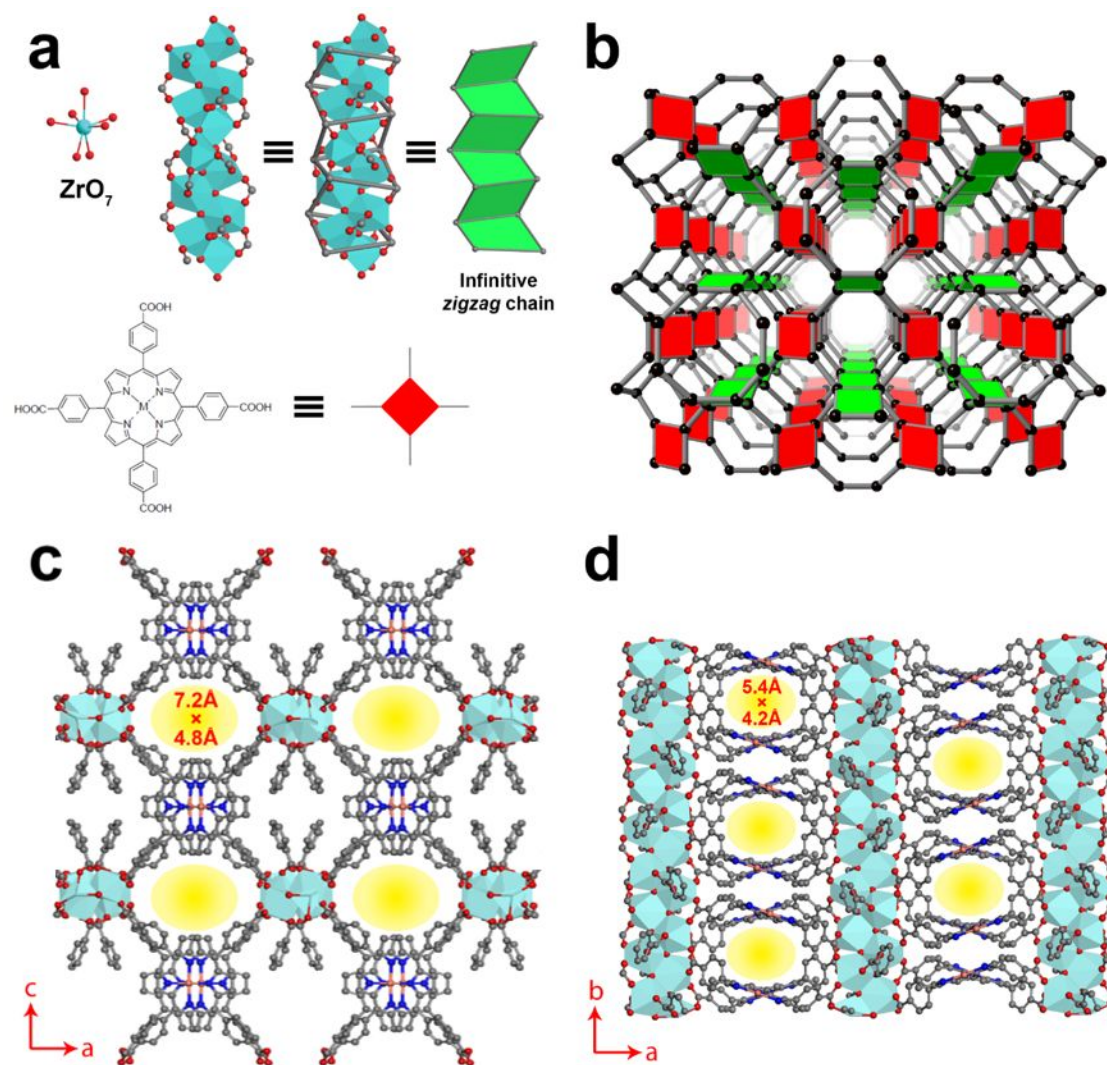


**Figure 2.** (a) PCN-226 is formed by the linkage of infinite zigzag zirconium chains and TCPP. The infinite zigzag zirconium chains have the composition [ZrO(-COO)<sub>2</sub>]<sub>∞</sub>, with Zr atoms being hepta-coordinated. (b) The connection of PCN-226 showing a new topology, with Schläfli symbol {4.8<sup>2</sup>} {4<sup>2</sup>.6.8<sup>2</sup>.10} for the net. (c) The crystal structure of PCN-226 viewed along the *b*-axis showing the pore opening 7.2 Å × 4.8 Å, and (d) the crystal structure viewed along the *c*-axis showing the 5.4 Å × 4.2 Å opening pores. Cyan capped octahedral: Zr; red spheres: O; black spheres: C; blue spheres: N; orange spheres: Cu.

**Table 1.** Comparison of the density of catalytically active-sites of PCN-226 with most reported porphyrinic Zr-MOFs.

Zr-metallo-porphyrin MOF	Building unit	Topology	Density ( $10^8$ porphyrinic metal sites $\mu\text{m}^{-3}$ ) <sup>[b]</sup>	Reference
PCN-226	ZrO <sub>7</sub> zigzag chain	New <sup>[a]</sup>	5.91	This work
PCN-221	Zr <sub>8</sub> ( $\mu_4$ -O) <sub>6</sub> cluster	<b>ftw</b>	4.04	51
MOF-525	Zr <sub>6</sub> ( $\mu_3$ -O) <sub>4</sub> ( $\mu_3$ -OH) <sub>4</sub> cluster	<b>ftw</b>	4.11	52
PCN-222	Zr <sub>6</sub> ( $\mu_3$ -OH) <sub>8</sub> cluster	<b>csq</b>	2.29	53
MOF-545	Zr <sub>6</sub> ( $\mu_3$ -O) <sub>8</sub> cluster	<b>csq</b>	2.28	52
PCN-223	Zr <sub>6</sub> ( $\mu_3$ -O) <sub>4</sub> ( $\mu_3$ -OH) <sub>4</sub> cluster	<b>shp</b>	4.47	54
PCN-224	Zr <sub>6</sub> ( $\mu_3$ -O) <sub>4</sub> ( $\mu_3$ -OH) <sub>4</sub> cluster	<b>she</b>	2.10	55
PCN-225	Zr <sub>6</sub> ( $\mu_3$ -O) <sub>4</sub> ( $\mu_3$ -OH) <sub>4</sub> cluster	<b>sqc</b>	3.72	56
PCN-228	Zr <sub>6</sub> ( $\mu_3$ -O) <sub>4</sub> ( $\mu_3$ -OH) <sub>4</sub> cluster	<b>ftw</b>	1.84	57
PCN-229	Zr <sub>6</sub> ( $\mu_3$ -O) <sub>4</sub> ( $\mu_3$ -OH) <sub>4</sub> cluster	<b>ftw</b>	1.37	57
PCN-230	Zr <sub>6</sub> ( $\mu_3$ -O) <sub>4</sub> ( $\mu_3$ -OH) <sub>4</sub> cluster	<b>ftw</b>	0.53	57
MMPF-6	Zr <sub>6</sub> ( $\mu_3$ -O) <sub>8</sub> cluster	<b>csq</b>	2.28	58

<sup>[a]</sup>The new topology of PCN-226 with Schlafli symbol  $\{4.8^2\}\{4^2.6.8^2.10\}$  for the net.

<sup>[b]</sup>The density was calculated based on the structural models.

Compared to the isolated clusters, the highly connected chain structures provide enhanced stability by resisting the attack of water and other guest species.<sup>49</sup> We tested chemical stabilities of PCN-226 using reported procedures in the MOF field.<sup>18,49</sup> It exhibited remarkable stabilities of PCN-226 in aqueous solutions in a wide pH range (1-13) for at least 7 days (Figures S13 and S14), as a result of the combination of chain structure and strong Zr(+4)–O bonding. PCN-226 showed very little leaching (< 0.97%) in acidic and basic conditions, as calculated from the UV-Vis spectra of PCN-226 measured at different pH values (pH 1-3 and 11-13) for 7 days (Figures S15-S18). Thermogravimetric analysis (TGA) showed PCN-226(Cu) was stable up to at least 400 °C (Figure S19). After the first weight loss before 100 °C due to the removal of guest molecules, only ~2% of the total framework weight was lost before the ligands starting combustion at above 400 °C. This shows the chain-containing PCN-226 is much more stable than the cluster-containing Zr-MOFs, which undergo dehydroxylation at a much lower temperature (~250 °C).<sup>29,45</sup>

### Electrocatalytic ORR of PCN-226.

PCN-226 provides an ideal example for designing MOF electrocatalysts through chain-based structures, which could improve the chemical stability as well as increase the packing density. A close packing could further enhance the overall charge mobility via hopping mechanism.<sup>30–32</sup> As a proof of concept, the electrochemical ORR catalyzed by PCN-226 was tested.

The isostructural PCN-226 series displayed excellent electroactivities towards ORR, which were assessed by cyclic voltammogram (CV) and linear sweep voltammetry (LSV) measurements (Figures S20, S21 and Table S5). As a 3D porous material, PCN-226 benefits from limited deactivation pathways compared to molecular catalysts (Figure S22). Given the best activity, PCN-226(Co) showed a strong reversible redox wave at 0.7 V (vs reversible hydrogen electrode, RHE, Figure 3a). The LSV curve of PCN-226(Co) (Figure 3b) exhibited an onset potential of 0.83 V ( $E_{\text{onset}}$ ) and half-wave potential of 0.75 V ( $E_{1/2}$ ), while the values of pure carbon black were 0.70 and 0.62 V, respectively (Figure S23). Meanwhile, PCN-226(H<sub>2</sub>) shows a very low activity with  $E_{1/2}$  of 0.6 V (vs RHE) (Figure S24). This

result highlights the importance of the metal cations in the porphyrin as they serve as the catalytic active sites. Notably, the potential can be further enhanced by increasing the catalyst loading (Figure S25). Due to the Zr-chain structure, the density of active metal sites in PCN-226 is so far the highest among reported porphyrinic Zr-MOFs, and it is 144% and 358% denser than the well-known PCN-221/MOF-525, and PCN-222/MOF-545, respectively (Table 1). The close packing increases the active-sites density as well as provides a better pathway for electron hopping. As a consequence, PCN-226 showed a better overall ORR activity than did by cluster-based MOFs PCN-221 ( $E_{1/2} = 0.70$  V vs. RHE) and PCN-222 ( $E_{1/2} = 0.69$  V vs. RHE) (Figures 3b, and Table S6). In addition, PCN-226 outperformed other commonly reported MOFs as ORR electrocatalysts, such as the MIL-88(Fe), ZIF-67(Co), MOF-5(Ni), and ZIF-8(Zn) (Figure S26).

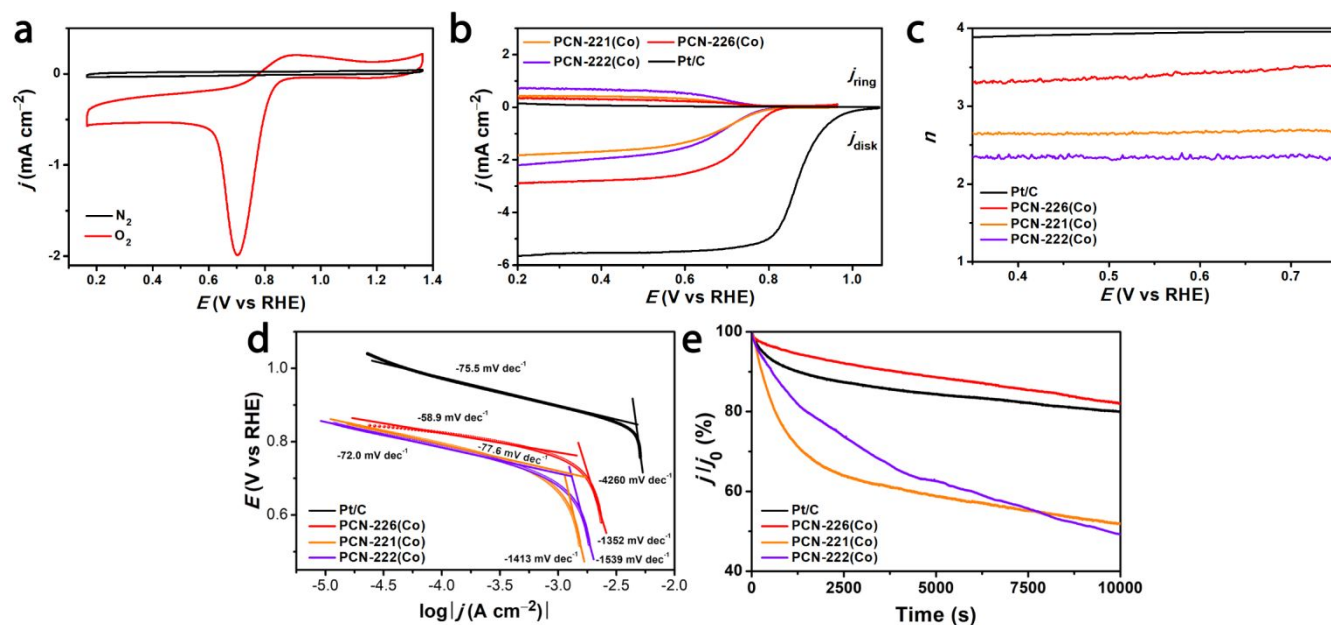


**Figure 3.** (a) CV curves of PCN-226(Co) in 0.1 M KOH solution saturated by  $N_2$  and  $O_2$ , respectively. (b) LSV curves, (c) electron transfer numbers ( $n$ ), and (d) Tafel plots of PCN-226(Co), PCN-221(Co), PCN-222(Co) and Pt/C. (e) Durability test at 0.46 V (vs. RHE) and 1600 rpm in  $O_2$ -saturated 0.1 M KOH solution,  $j_0$  is the initial current. It shows PCN-226(Co) has the lowest current loss (18%), followed by Pt/C (20%), PCN-221(Co) (48%), and PCN-222(Co) (50%). The MOFs were mixed with 50% carbon black.

Electrocatalytic ORR can be carried out in an alkaline solution through four electron ( $4e^-$ ) and two electron ( $2e^-$ ) pathways. Notably, the  $4e^-$  selectivity provides higher reaction kinetics and can prolong the durability of the cell. The electron transfer number ( $n$ ) of PCN-226(Co) was calculated as  $\sim 3.3$ , which indicated a mixed  $4e^-$  and  $2e^-$  pathways. Compared with the  $n$  number of Zr-cluster based PCN-221 (2.6) and PCN-222 (2.3), as well as pure carbon black (2.1), PCN-226(Co) offers a better reaction pathway towards the reduction of  $O_2$  to  $OH^-$  (Figures 3c and S27, see Supporting Information for more details). Although the  $n$  number of PCN-226(Co) was slightly lower than that (3.9) observed for Pt/C, PCN-226(Co) provided a faster reaction kinetics as shown by the Tafel slopes (Figure 3d). As expected from the close spacing of active-sites, the reaction kinetics of PCN-226 was the fastest among the porphyrinic Zr-MOFs we tested (Figure 3d, see Supporting Information). The calculated turnover frequency (TOF) of PCN-226(Co) at 0.2 V (vs RHE) is  $0.17 \text{ e site}^{-1} \text{ s}^{-1}$ , assuming all the Co atoms on the electrode are available. This TOF is comparable with that of Pt/C ( $0.18 \text{ e site}^{-1} \text{ s}^{-1}$ ) and other reported materials (Table S7). Furthermore, by limiting deactivation pathways, PCN-226(Co) endowed



a superior tolerance to methanol crossover (Figure S28). PCN-226(Co) exhibited a high durability with the lowest current loss of 18%, especially compared to the other cluster-based MOFs (Figures 3e and S29). After the durability test, structural and compositional measurements confirmed that PCN-226(Co) remained intact, without decomposition or generation of metal oxides (Figures S30-S32).

We further evaluated the OER activity (Figure S33, see Supporting Information for more details), and used PCN-226(Co) as air electrodes for practical applications in a rechargeable Zn-air battery (Figures 4a, S34 and Movie S1). By coating the catalysts on carbon cloth to further enhance electron transfer,<sup>59</sup> the assembled battery exhibited an open-circuit voltage of 1.37 V (Figure S35), and the discharge and charge voltage were 1.17 and 2.14 V, respectively (Figure 4b). The specific capacity of PCN-226(Co) was 724 mAh g<sup>-1</sup>, which is close to 757 mAh g<sup>-1</sup> using Pt/C+RuO<sub>2</sub> catalysts (Figure 4c). We further compared the peak power density, which is one of critical metrics for practical applications, with other electrodes. The peak power density of PCN-226(Co) was 133 mW cm<sup>-2</sup>, which was comparable to the 150 mW cm<sup>-2</sup> observed for Pt/C+RuO<sub>2</sub> (Figure 4d), and exceeded those for the previously reported state-of-the-art noble metal-free electrocatalysts, such as MOFs and MOF derived composites,<sup>60–64</sup> carbon materials,<sup>11,65–69</sup> and metal oxide composites<sup>70–72</sup> (Table S8). Significantly, no noticeable performance decrease was observed after 550 charge-discharge cycles over 160 h, indicating a high electrocatalytic durability (Figure 4e).

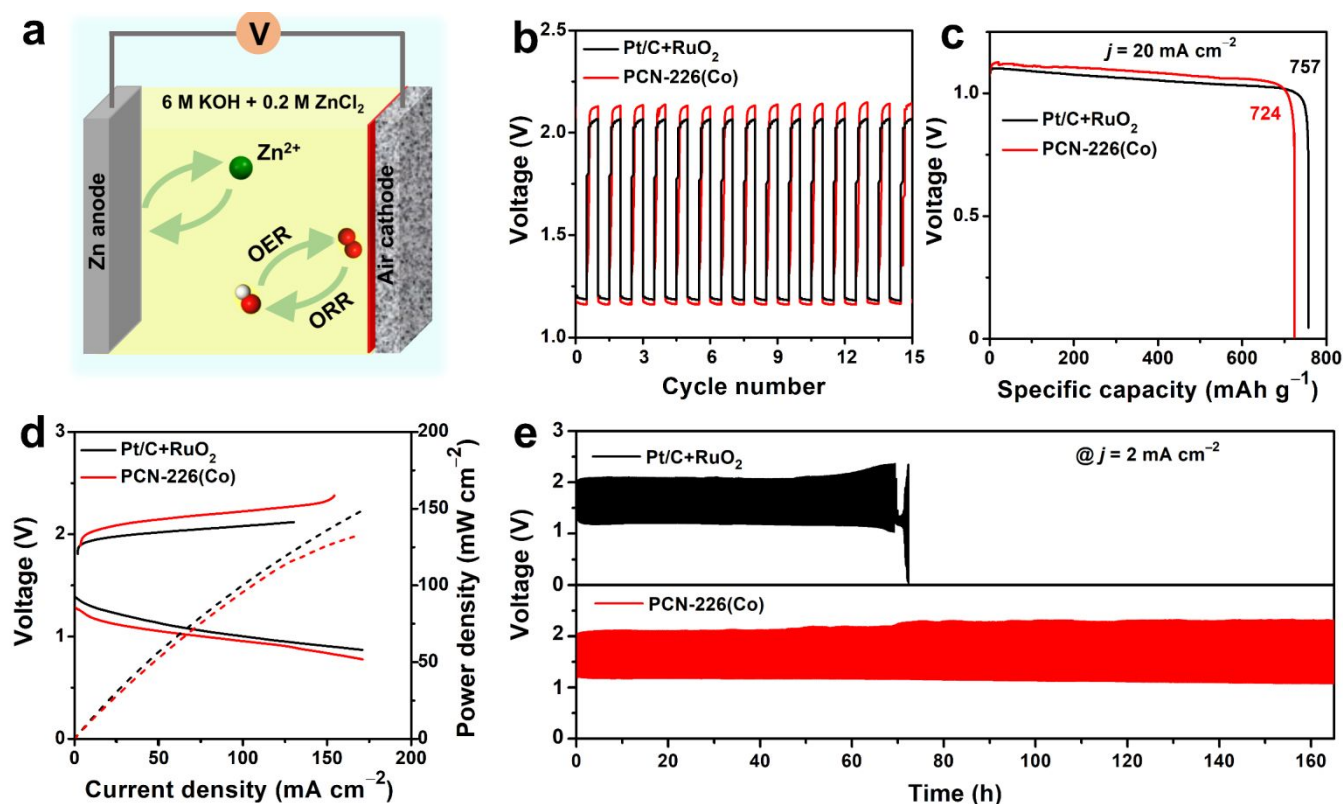


**Figure 4.** (a) Schematic illustration of the Zn-air battery. (b) Discharge and charge cycling curves. (c) Discharging curves at  $j = 20 \text{ mA cm}^{-2}$ . (d) Polarization curves and corresponding power density. (e) Long-term durability test of Zn-air batteries at  $j = 2 \text{ mA cm}^{-2}$  assembled with PCN-226(Co) and commercial Pt/C+RuO<sub>2</sub>. The loading of PCN-226(Co) is 6.25 times as it was used in ORR test.

### Theoretical calculation.

As we demonstrated above, a highly dense structure could improve the performance through high catalyst loading as well as enhanced charge transfer. Single metal atom catalysts, which readily bind to the reaction intermediates of ORR are an extreme example with infinite distance between active-sites. As shown below, tuning the spacing between two single metal atom active-sites becomes extremely crucial for optimizing both the density of the active-sites and the reaction thermodynamics, which in turn affects the reaction kinetics. The central key is to engineer the spacing so that the binding energies of ORR intermediates, i.e.,  $\text{OOH}^*$ ,  $\text{O}^*$  and  $\text{OH}^*$  are neither too strong nor too weak. This design leads to the minimum overpotential as well as high intrinsic ORR catalytic activity.<sup>73</sup> To demonstrate this effect, we studied the confinement in the Co-porphyrin sites of PCN-226 using a truncated model with the same atomic coordination (Figure 5a). PCN-226 has two inherent confined spacings between the porphyrin units i.e., 4 Å and 7 Å. In addition to the natural spacings in PCN-226, we considered several other spacings to investigate the effect of confinement on the ORR activity. The calculated adsorption free energies ( $\Delta G$ ) of ORR intermediates ( $\text{O}^*$ ,  $\text{OH}^*$ ,  $\text{OOH}^*$ ) at different spacings are displayed in Figure 5b. The results show that at 4 Å spacing all ORR intermediates are significantly destabilized indicating that this spacing is less probable to contribute to the observed ORR activity. On the other hand, all  $\Delta G$  values approach those of an ideal catalyst for spacings larger than 6 Å. The ideal spacing for  $\Delta G_{\text{OOH}}$  is between 6 Å to 8 Å. Combined with the highly dense chain structure, this spacing explains the enhanced ORR activity observed in the case of our PCN-226 catalyst with well-defined 7 Å spacing. We further examined the effect of curvature on the ORR activity by examining a flattened model of the Co-porphyrins with 7 Å spacing, where we found negligible differences in the  $\Delta G$  values of roughly 0.05 eV. The calculation results signify the importance of the spacing of active-sites on the performance in ORR.

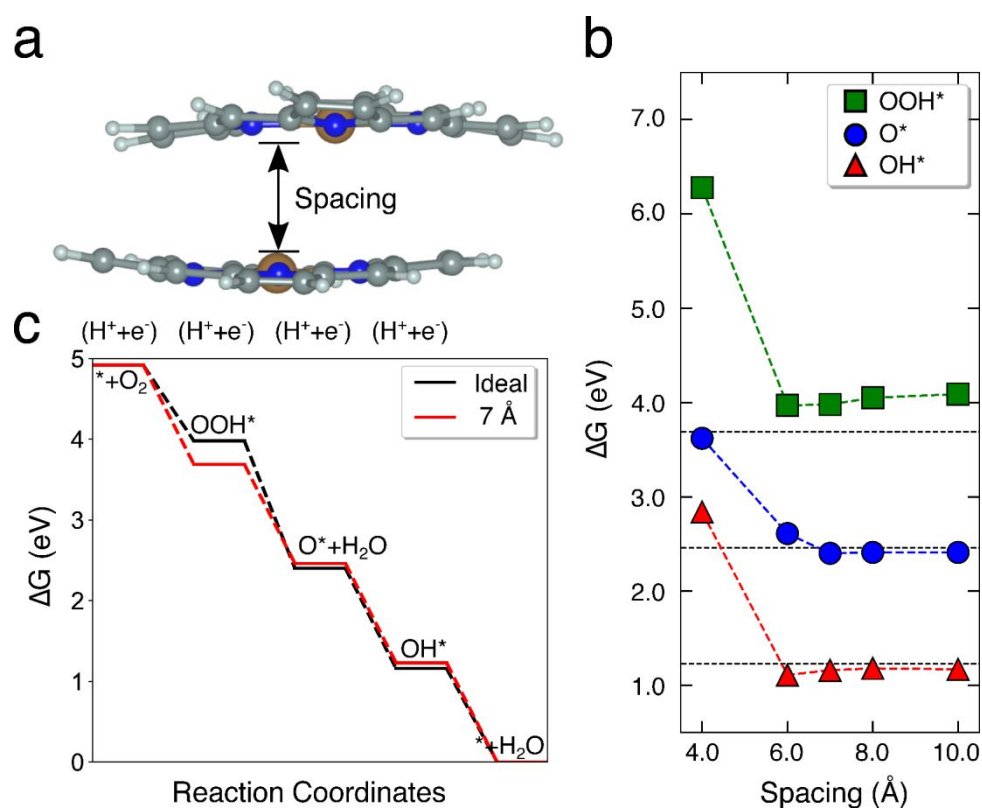


**Figure 5.** (a) A truncated molecular model of PCN-226. Color code; brown: Co; blue: N; grey: C; white: H. We varied the distance between two porphyrin motifs to investigate the effect of the spacing on ORR. (b) Adsorption

free energy of ORR intermediates as a function of the spacing. The two inherent spacings in PCN-226 are ca. 4 and 7 Å. The horizontal dashed lines indicate  $\Delta G$  of an ideal catalyst. (c) Free energy diagram for the 7 Å spacing between porphyrin motifs (red) compared with the ideal catalyst (black).

## CONCLUSIONS

We developed a new Zr oxide-chain based MOF, PCN-226. Metalloporphyrin was incorporated in the framework, which can act as redox active catalyst. PCN-226 demonstrates an excellent chemical stability, which enforces its compatibility in aqueous solution as electrocatalysts. We present a proof-of-concept study that highlights the importance of chain-based 3D structure in MOF design for electrochemical applications. In particular, chain-based MOFs not only allow the incorporation of close-packed, high-density redox-active-sites, but also provide an opportunity to tailor the spacing between those active-sites. Thanks to this strategy, PCN-226 shows excellent electroactivity compared with that of cluster-based MOFs. We foresee the tunability and designability in MOF structures will promote future development on chain-based 3D MOFs as electrocatalysts. Such developments will further close the gap between reticular chemistry and materials catalysis, particularly in electrocatalysis, which contribute significantly to green energy conversion and storage.

## ASSOCIATED CONTENT

### Supporting Information

The crystallographic data for PCN-226(Cu) and PCN-226(Co) have been deposited at the Cambridge Crystallographic Data Centre (CCDC, free for charge at <https://www.ccdc.cam.ac.uk>) under deposition number CCDC 2004306, and 2020844, respectively. The Supporting Information is available free of charge on the ACS Publications website at DOI:.

Experimental details, PXRD, gas sorption, SEM, ICP-OES, structure refinement, XPS, electrocatalytic O<sub>2</sub> reduction, and DFT calculations (PDF)

Crystallographic information files for PCN-226(Cu) and PCN-226(Co) (CIF)

Movie S1: Recording of a Zn-air battery powered mini car using PCN-226 as air electrodes (MP4)

## AUTHOR INFORMATION

### Corresponding Author

\*(H.Z.) E-mail: zhenghaoquan@snnu.edu.cn.

\*(H.-C.Z.) E-mail: zhou@chem.tamu.edu.

\*(Z.H.) E-mail: zhehao.huang@mmk.su.se.

### Author Contributions

†M. O. Cichocka, and Z. Liang contributed equally to this work.

### Notes

The authors declare no competing interests.

## ACKNOWLEDGMENT

This research was supported by the Swedish Research Council (VR, 2016-04625, 2017-04321), the CATSS project from the Knut and Alice Wallenberg Foundation (KAW, 2016.0072), and National Natural Science Foundation of China (Grant No. 21975148, 21808138, and 21601118). S.S. acknowledges the support from the University of Calgary's Canada First Research Excellence Fund Program, the Global Research Initiative in Sustainable Low Carbon Unconventional Resources.

## REFERENCES

- (1) Shao, M.; Chang, Q.; Dodelet, J.-P.; Chenitz, R. Recent Advances in Electrocatalysts for Oxygen Reduction Reaction. *Chem. Rev.* **2016**, *116* (6), 3594–3657.
- (2) Cheng, F.; Chen, J. Metal–Air Batteries: From Oxygen Reduction Electrochemistry to Cathode Catalysts. *Chem. Soc. Rev.* **2012**, *41* (6), 2172–2192.

- (3) Wang, Y.-J.; Zhao, N.; Fang, B.; Li, H.; Bi, X. T.; Wang, H. Carbon-Supported Pt-Based Alloy Electrocatalysts for the Oxygen Reduction Reaction in Polymer Electrolyte Membrane Fuel Cells: Particle Size, Shape, and Composition Manipulation and Their Impact to Activity. *Chem. Rev.* **2015**, *115* (9), 3433–3467.
- (4) Chen, Z.; Higgins, D.; Yu, A.; Zhang, L.; Zhang, J. A Review on Non-Precious Metal Electrocatalysts for PEM Fuel Cells. *Energy Environ. Sci.* **2011**, *4* (9), 3167–3192.
- (5) Nie, Y.; Li, L.; Wei, Z. Recent Advancements in Pt and Pt-Free Catalysts for Oxygen Reduction Reaction. *Chem. Soc. Rev.* **2015**, *44* (8), 2168–2201.
- (6) Hou, J.; Wu, Y.; Zhang, B.; Cao, S.; Li, Z.; Sun, L. Rational Design of Nanoarray Architectures for Electrocatalytic Water Splitting. *Adv. Funct. Mater.* **2019**, *29* (20), 1808367.
- (7) Liang, Z.; Fan, X.; Lei, H.; Qi, J.; Li, Y.; Gao, J.; Huo, M.; Yuan, H.; Zhang, W.; Lin, H.; Zheng, H.; Cao, R. Cobalt–Nitrogen-Doped Helical Carbonaceous Nanotubes as a Class of Efficient Electrocatalysts for the Oxygen Reduction Reaction. *Angew. Chem. Int. Ed.* **2018**, *57* (40), 13187–13191.
- (8) Zhang, C.; Yang, H.; Zhong, D.; Xu, Y.; Wang, Y.; Yuan, Q.; Liang, Z.; Wang, B.; Zhang, W.; Zheng, H.; Cheng, T.; Cao, R. A Yolk–Shell Structured Metal–Organic Framework with Encapsulated Iron–Porphyrin and Its Derived Bimetallic Nitrogen-Doped Porous Carbon for an Efficient Oxygen Reduction Reaction. *J. Mater. Chem. A* **2020**, *8* (19), 9536–9544.
- (9) Yaghi, O. M.; O’Keeffe, M.; Ockwig, N. W.; Chae, H. K.; Eddaoudi, M.; Kim, J. Reticular Synthesis and the Design of New Materials. *Nature* **2003**, *423* (6941), 705–714.
- (10) Kitagawa, S.; Kitaura, R.; Noro, S. Functional Porous Coordination Polymers. *Angew. Chem. Int. Ed.* **2004**, *43* (18), 2334–2375.
- (11) Yang, S.; Yu, Y.; Dou, M.; Zhang, Z.; Dai, L.; Wang, F. Two-Dimensional Conjugated Aromatic Networks as High-Site-Density and Single-Atom Electrocatalysts for the Oxygen Reduction Reaction. *Angew. Chem. Int. Ed.* **2019**, *58* (41), 14724–14730.
- (12) Zion, N.; Cullen, D. A.; Zelenay, P.; Elbaz, L. Heat-Treated Aerogel as a Catalyst for the Oxygen Reduction Reaction. *Angew. Chem. Int. Ed.* **2020**, *59* (6), 2483–2489.
- (13) Eddaoudi, M.; Kim, J.; Rosi, N.; Vodak, D.; Wachter, J.; O’Keeffe, M.; Yaghi, O. M. Systematic Design of Pore Size and Functionality in Isoreticular MOFs and Their Application in Methane Storage. *Science* **2002**, *295* (5554), 469–472.
- (14) Aijaz, A.; Fujiwara, N.; Xu, Q. From Metal–Organic Framework to Nitrogen-Decorated Nanoporous Carbons: High CO<sub>2</sub> Uptake and Efficient Catalytic Oxygen Reduction. *J. Am. Chem. Soc.* **2014**, *136* (19), 6790–6793.
- (15) Xia, B. Y.; Yan, Y.; Li, N.; Wu, H. B.; Lou, X. W. (David); Wang, X. A Metal–Organic Framework-Derived Bifunctional Oxygen Electrocatalyst. *Nat. Energy* **2016**, *1* (1), 15006.
- (16) Yang, F.; Xu, G.; Dou, Y.; Wang, B.; Zhang, H.; Wu, H.; Zhou, W.; Li, J.-R.; Chen, B. A Flexible Metal–Organic Framework with a High Density of Sulfonic Acid Sites for Proton Conduction. *Nat. Energy* **2017**, *2* (11), 877.
- (17) Yu, X.; Wang, L.; Cohen, S. M. Photocatalytic Metal–Organic Frameworks for Organic Transformations. *CrystEngComm* **2017**, *19* (29), 4126–4136.
- (18) Yuan, S.; Qin, J.-S.; Xu, H.-Q.; Su, J.; Rossi, D.; Chen, Y.; Zhang, L.; Lollar, C.; Wang, Q.; Jiang, H.-L.; Son, D. H.; Xu, H.; Huang, Z.; Zou, X.; Zhou, H.-C. [Ti<sub>8</sub>Zr<sub>2</sub>O<sub>12</sub>(COO)<sub>16</sub>] Cluster: An Ideal Inorganic Building Unit for Photoactive Metal–Organic Frameworks. *ACS Cent. Sci.* **2018**, *4* (1), 105–111.
- (19) Jiao, L.; Wan, G.; Zhang, R.; Zhou, H.; Yu, S.-H.; Jiang, H.-L. From Metal–Organic Frameworks to Single-Atom Fe Implanted N-Doped Porous Carbons: Efficient Oxygen Reduction in Both Alkaline and Acidic Media. *Angew. Chem. Int. Ed.* **2018**, *57* (28), 8525–8529.
- (20) Hou, C.-C.; Zou, L.; Sun, L.; Zhang, K.; Liu, Z.; Li, Y.; Li, C.; Zou, R.; Yu, J.; Xu, Q. Single-Atom Iron Catalysts on Overhang-Eave Carbon Cages for High-Performance Oxygen Reduction Reaction. *Angew. Chem. Int. Ed.* **2020**, *59* (19), 7384–7389.
- (21) Sheberla, D.; Bachman, J. C.; Elias, J. S.; Sun, C.-J.; Shao-Horn, Y.; Dincă, M. Conductive MOF Electrodes for Stable Supercapacitors with High Areal Capacitance. *Nat. Mater.* **2017**, *16* (2), 220–224.
- (22) Feng, D.; Lei, T.; Lukatskaya, M. R.; Park, J.; Huang, Z.; Lee, M.; Shaw, L.; Chen, S.; Yakovenko, A. A.; Kulkarni, A.; Xiao, J.; Fredrickson, K.; Tok, J. B.; Zou, X.; Cui, Y.; Bao, Z. Robust and Conductive Two-Dimensional Metal–organic Frameworks with Exceptionally High Volumetric and Areal Capacitance. *Nat. Energy* **2018**, *3* (1), 30–36.
- (23) Park, J.; Hinckley, A. C.; Huang, Z.; Feng, D.; Yakovenko, A. A.; Lee, M.; Chen, S.; Zou, X.; Bao, Z. Synthetic Routes for a 2D Semiconductive Copper Hexahydroxybenzene Metal–Organic Framework. *J. Am. Chem. Soc.* **2018**, *140* (44), 14533–14537.

- (24) Park, J.; Lee, M.; Feng, D.; Huang, Z.; Hinckley, A. C.; Yakovenko, A.; Zou, X.; Cui, Y.; Bao, Z. Stabilization of Hexaaminobenzene in a 2D Conductive Metal–Organic Framework for High Power Sodium Storage. *J. Am. Chem. Soc.* **2018**, *140* (32), 10315–10323.
- (25) Day, R. W.; Bediako, D. K.; Rezaee, M.; Parent, L. R.; Skorupskii, G.; Arguilla, M. Q.; Hendon, C. H.; Stassen, I.; Gianneschi, N. C.; Kim, P.; Dincă, M. Single Crystals of Electrically Conductive Two-Dimensional Metal–Organic Frameworks: Structural and Electrical Transport Properties. *ACS Cent. Sci.* **2019**, *5* (12), 1959–1964.
- (26) Yao, M.-S.; Zheng, J.-J.; Wu, A.-Q.; Xu, G.; Nagarkar, S. S.; Zhang, G.; Tsujimoto, M.; Sakaki, S.; Horike, S.; Otake, K.; Kitagawa, S. A Dual-Ligand Porous Coordination Polymer Chemiresistor with Modulated Conductivity and Porosity. *Angew. Chem. Int. Ed.* **2020**, *59* (1), 172–176.
- (27) Wang, T. C.; Hod, I.; Audu, C. O.; Vermeulen, N. A.; Nguyen, S. T.; Farha, O. K.; Hupp, J. T. Rendering High Surface Area, Mesoporous Metal–Organic Frameworks Electronically Conductive. *ACS Appl. Mater. Interfaces* **2017**, *9* (14), 12584–12591.
- (28) Stassen, I.; Burtch, N.; Talin, A.; Falcaro, P.; Allendorf, M.; Ameloot, R. An Updated Roadmap for the Integration of Metal–Organic Frameworks with Electronic Devices and Chemical Sensors. *Chem. Soc. Rev.* **2017**, *46* (11), 3185–3241.
- (29) Roy, S.; Huang, Z.; Bhunia, A.; Castner, A.; Gupta, A. K.; Zou, X.; Ott, S. Electrocatalytic Hydrogen Evolution from a Cobaloxime-Based Metal–Organic Framework Thin Film. *J. Am. Chem. Soc.* **2019**, *141* (40), 15942–15950.
- (30) AlKaabi, K.; Wade, C. R.; Dincă, M. Transparent-to-Dark Electrochromic Behavior in Naphthalene-Diimide-Based Mesoporous MOF-74 Analogs. *Chem* **2016**, *1* (2), 264–272.
- (31) Ahrenholtz, S. R.; Epley, C. C.; Morris, A. J. Solvothermal Preparation of an Electrocatalytic Metalloporphyrin MOF Thin Film and Its Redox Hopping Charge-Transfer Mechanism. *J. Am. Chem. Soc.* **2014**, *136* (6), 2464–2472.
- (32) Liberman, I.; Shimon, R.; Ifraimov, R.; Rozenberg, I.; Singh, C.; Hod, I. Active-Site Modulation in an Fe-Porphyrin-Based Metal–Organic Framework through Ligand Axial Coordination: Accelerating Electrocatalysis and Charge-Transport Kinetics. *J. Am. Chem. Soc.* **2020**, *142* (4), 1933–1940.
- (33) Fateeva, A.; Chater, P. A.; Ireland, C. P.; Tahir, A. A.; Khimyak, Y. Z.; Wiper, P. V.; Darwent, J. R.; Rosseinsky, M. J. A Water-Stable Porphyrin-Based Metal–Organic Framework Active for Visible-Light Photocatalysis. *Angew. Chem. Int. Ed.* **2012**, *51* (30), 7440–7444.
- (34) Micheroni, D.; Lan, G.; Lin, W. Efficient Electrocatalytic Proton Reduction with Carbon Nanotube-Supported Metal–Organic Frameworks. *J. Am. Chem. Soc.* **2018**, *140* (46), 15591–15595.
- (35) Kornienko, N.; Zhao, Y.; Kley, C. S.; Zhu, C.; Kim, D.; Lin, S.; Chang, C. J.; Yaghi, O. M.; Yang, P. Metal–Organic Frameworks for Electrocatalytic Reduction of Carbon Dioxide. *J. Am. Chem. Soc.* **2015**, *137* (44), 14129–14135.
- (36) Dong, B.-X.; Qian, S.-L.; Bu, F.-Y.; Wu, Y.-C.; Feng, L.-G.; Teng, Y.-L.; Liu, W.-L.; Li, Z.-W. Electrochemical Reduction of CO<sub>2</sub> to CO by a Heterogeneous Catalyst of Fe–Porphyrin-Based Metal–Organic Framework. *ACS Appl. Energy Mater.* **2018**, *1* (9), 4662–4669.
- (37) Hod, I.; Sampson, M. D.; Deria, P.; Kubiak, C. P.; Farha, O. K.; Hupp, J. T. Fe-Porphyrin-Based Metal–Organic Framework Films as High-Surface Concentration, Heterogeneous Catalysts for Electrochemical Reduction of CO<sub>2</sub>. *ACS Catal.* **2015**, *5* (11), 6302–6309.
- (38) Lu, X.-F.; Liao, P.-Q.; Wang, J.-W.; Wu, J.-X.; Chen, X.-W.; He, C.-T.; Zhang, J.-P.; Li, G.-R.; Chen, X.-M. An Alkaline-Stable, Metal Hydroxide Mimicking Metal–Organic Framework for Efficient Electrocatalytic Oxygen Evolution. *J. Am. Chem. Soc.* **2016**, *138* (27), 8336–8339.
- (39) Xue, Z.; Liu, K.; Liu, Q.; Li, Y.; Li, M.; Su, C.-Y.; Ogiwara, N.; Kobayashi, H.; Kitagawa, H.; Liu, M.; Li, G. Missing-Linker Metal–Organic Frameworks for Oxygen Evolution Reaction. *Nat. Commun.* **2019**, *10* (1), 5048.
- (40) Li, W.; Xue, S.; Watzele, S.; Hou, S.; Fichtner, J.; Semrau, A. L.; Zhou, L.; Welle, A.; Bandarenka, A. S.; Fischer, R. A. Advanced Bifunctional Oxygen Reduction and Evolution Electrocatalyst Derived from Surface-Mounted Metal–Organic Frameworks. *Angew. Chem. Int. Ed.* **2020**, *59* (14), 5837–5843.
- (41) Usov, P. M.; Huffman, B.; Epley, C. C.; Kessinger, M. C.; Zhu, J.; Maza, W. A.; Morris, A. J. Study of Electrocatalytic Properties of Metal–Organic Framework PCN-223 for the Oxygen Reduction Reaction. *ACS Appl. Mater. Interfaces* **2017**, *9* (39), 33539–33543.
- (42) Cheng, W.; Zhao, X.; Su, H.; Tang, F.; Che, W.; Zhang, H.; Liu, Q. Lattice-Strained Metal–Organic-Framework Arrays for Bifunctional Oxygen Electrocatalysis. *Nat. Energy* **2019**, *4* (2), 115–122.
- (43) Zhong, H.; Ly, K. H.; Wang, M.; Krupskaya, Y.; Han, X.; Zhang, J.; Zhang, J.; Kataev, V.; Büchner, B.; Weidinger, I. M.; Kaskel, S.; Liu, P.; Chen, M.; Dong, R.; Feng, X. A Phthalocyanine-Based Layered Two-Dimensional Conjugated Metal–Organic Framework as a Highly Efficient Electrocatalyst for the Oxygen Reduction Reaction. *Angew. Chem. Int. Ed.* **2019**, *58* (31), 10677–10682.



- (44) Lu, X. F.; Xia, B. Y.; Zang, S.-Q.; Lou, X. W. (David). Metal–Organic Frameworks Based Electrocatalysts for the Oxygen Reduction Reaction. *Angew. Chem. Int. Ed.* **2020**, *59* (12), 4634–4650.
- (45) Cavka, J. H.; Jakobsen, S.; Olsbye, U.; Guillou, N.; Lamberti, C.; Bordiga, S.; Lillerud, K. P. A New Zirconium Inorganic Building Brick Forming Metal Organic Frameworks with Exceptional Stability. *J. Am. Chem. Soc.* **2008**, *130* (42), 13850–13851.
- (46) Cichocka, M. O.; Ångström, J.; Wang, B.; Zou, X.; Smeets, S. High-Throughput Continuous Rotation Electron Diffraction Data Acquisition via Software Automation. *J. Appl. Crystallogr.* **2018**, *51* (6), 1652–1661.
- (47) Huang, Z.; Ge, M.; Carraro, F.; Doonan, C. J.; Falcaro, P.; Zou, X. Can 3D Electron Diffraction Provide Accurate Atomic Structures of Metal–Organic Frameworks? *Faraday Discuss.* **2020**. DOI: 10.1039/D0FD00015A.
- (48) Warren, M. ‘Why Didn’t We Think to Do This Earlier?’ Chemists Thrilled by Speedy Atomic Structures. *Nature* **2018**, *563*, 16.
- (49) Guillermin, V.; Ragon, F.; Dan-Hardi, M.; Devic, T.; Vishnuvarthan, M.; Campo, B.; Vimont, A.; Clet, G.; Yang, Q.; Maurin, G.; Férey, G.; Vittadini, A.; Gross, S.; Serre, C. A Series of Isorecticular, Highly Stable, Porous Zirconium Oxide Based Metal–Organic Frameworks. *Angew. Chem. Int. Ed.* **2012**, *51* (37), 9267–9271.
- (50) Mouchaham, G.; Cooper, L.; Guillou, N.; Martineau, C.; Elkaïm, E.; Bourrelly, S.; Llewellyn, P. L.; Allain, C.; Clavier, G.; Serre, C.; Devic, T. A Robust Infinite Zirconium Phenolate Building Unit to Enhance the Chemical Stability of Zr MOFs. *Angew. Chem. Int. Ed.* **2015**, *54* (45), 13297–13301.
- (51) Feng, D.; Jiang, H.-L.; Chen, Y.-P.; Gu, Z.-Y.; Wei, Z.; Zhou, H.-C. Metal–Organic Frameworks Based on Previously Unknown Zr<sub>8</sub>/Hf<sub>8</sub> Cubic Clusters. *Inorg. Chem.* **2013**, *52* (21), 12661–12667.
- (52) Morris, W.; Voloskiy, B.; Demir, S.; Gándara, F.; McGrier, P. L.; Furukawa, H.; Cascio, D.; Stoddart, J. F.; Yaghi, O. M. Synthesis, Structure, and Metalation of Two New Highly Porous Zirconium Metal–Organic Frameworks. *Inorg. Chem.* **2012**, *51* (12), 6443–6445.
- (53) Feng, D.; Gu, Z.-Y.; Li, J.-R.; Jiang, H.-L.; Wei, Z.; Zhou, H.-C. Zirconium-Metalloporphyrin PCN-222: Mesoporous Metal–Organic Frameworks with Ultrahigh Stability as Biomimetic Catalysts. *Angew. Chem. Int. Ed.* **2012**, *51* (41), 10307–10310.
- (54) Feng, D.; Gu, Z.-Y.; Chen, Y.-P.; Park, J.; Wei, Z.; Sun, Y.; Bosch, M.; Yuan, S.; Zhou, H.-C. A Highly Stable Porphyrinic Zirconium Metal–Organic Framework with Shp-a Topology. *J. Am. Chem. Soc.* **2014**, *136* (51), 17714–17717.
- (55) Feng, D.; Chung, W.-C.; Wei, Z.; Gu, Z.-Y.; Jiang, H.-L.; Chen, Y.-P.; Darensbourg, D. J.; Zhou, H.-C. Construction of Ultrastable Porphyrin Zr Metal–Organic Frameworks through Linker Elimination. *J. Am. Chem. Soc.* **2013**, *135* (45), 17105–17110.
- (56) Jiang, H.-L.; Feng, D.; Wang, K.; Gu, Z.-Y.; Wei, Z.; Chen, Y.-P.; Zhou, H.-C. An Exceptionally Stable, Porphyrinic Zr Metal–Organic Framework Exhibiting PH-Dependent Fluorescence. *J. Am. Chem. Soc.* **2013**, *135* (37), 13934–13938.
- (57) Liu, T.-F.; Feng, D.; Chen, Y.-P.; Zou, L.; Bosch, M.; Yuan, S.; Wei, Z.; Fordham, S.; Wang, K.; Zhou, H.-C. Topology-Guided Design and Syntheses of Highly Stable Mesoporous Porphyrinic Zirconium Metal–Organic Frameworks with High Surface Area. *J. Am. Chem. Soc.* **2015**, *137* (1), 413–419.
- (58) Chen, Y.; Hoang, T.; Ma, S. Biomimetic Catalysis of a Porous Iron-Based Metal–Metalloporphyrin Framework. *Inorg. Chem.* **2012**, *51* (23), 12600–12602.
- (59) Shi, H.; Wen, G.; Nie, Y.; Zhang, G.; Duan, H. Flexible 3D Carbon Cloth as a High-Performing Electrode for Energy Storage and Conversion. *Nanoscale* **2020**, *12* (9), 5261–5285.
- (60) Chen, G.; Zhang, J.; Wang, F.; Wang, L.; Liao, Z.; Zschech, E.; Müllen, K.; Feng, X. Cobalt-Based Metal–Organic Framework Nanoarrays as Bifunctional Oxygen Electrocatalysts for Rechargeable Zn–Air Batteries. *Chem. – Eur. J.* **2018**, *24* (69), 18413–18418.
- (61) Kang, X.; Fu, G.; Song, Z.; Huo, G.; Si, F.; Deng, X.; Fu, X.-Z.; Luo, J.-L. Microwave-Assisted Hydrothermal Synthesis of MOFs-Derived Bimetallic CuCo–N/C Electrocatalyst for Efficient Oxygen Reduction Reaction. *J. Alloys Compd.* **2019**, *795*, 462–470.
- (62) Zhao, J.-Y.; Wang, R.; Wang, S.; Lv, Y.-R.; Xu, H.; Zang, S.-Q. Metal–Organic Framework-Derived Co<sub>9</sub>S<sub>8</sub> Embedded in N, O and S-Tridoped Carbon Nanomaterials as an Efficient Oxygen Bifunctional Electrocatalyst. *J. Mater. Chem. A* **2019**, *7* (13), 7389–7395.
- (63) Zhong, Y.; Pan, Z.; Wang, X.; Yang, J.; Qiu, Y.; Xu, S.; Lu, Y.; Huang, Q.; Li, W. Hierarchical Co<sub>3</sub>O<sub>4</sub> Nano-Micro Arrays Featuring Superior Activity as Cathode in a Flexible and Rechargeable Zinc–Air Battery. *Adv. Sci.* **2019**, *6* (11), 1802243.
- (64) Cai, Z.; Yamada, I.; Yagi, S. ZIF-Derived Co<sub>9</sub>–XNi<sub>x</sub>S<sub>8</sub> Nanoparticles Immobilized on N-Doped Carbons as Efficient Catalysts for High-Performance Zinc–Air Batteries. *ACS Appl. Mater. Interfaces* **2020**, *12* (5), 5847–5856.

- (65) Zhang, J.; Zhao, Z.; Xia, Z.; Dai, L. A Metal-Free Bifunctional Electrocatalyst for Oxygen Reduction and Oxygen Evolution Reactions. *Nat. Nanotechnol.* **2015**, *10* (5), 444–452.
- (66) Yang, H. B.; Miao, J.; Hung, S.-F.; Chen, J.; Tao, H. B.; Wang, X.; Zhang, L.; Chen, R.; Gao, J.; Chen, H. M.; Dai, L.; Liu, B. Identification of Catalytic Sites for Oxygen Reduction and Oxygen Evolution in N-Doped Graphene Materials: Development of Highly Efficient Metal-Free Bifunctional Electrocatalyst. *Sci. Adv.* **2016**, *2* (4), e1501122.
- (67) Hu, Q.; Li, G.; Li, G.; Liu, X.; Zhu, B.; Chai, X.; Zhang, Q.; Liu, J.; He, C. Trifunctional Electrocatalysis on Dual-Doped Graphene Nanorings–Integrated Boxes for Efficient Water Splitting and Zn–Air Batteries. *Adv. Energy Mater.* **2019**, *9* (14), 1803867.
- (68) Chen, P.; Zhou, T.; Xing, L.; Xu, K.; Tong, Y.; Xie, H.; Zhang, L.; Yan, W.; Chu, W.; Wu, C.; Xie, Y. Atomically Dispersed Iron–Nitrogen Species as Electrocatalysts for Bifunctional Oxygen Evolution and Reduction Reactions. *Angew. Chem. Int. Ed.* **2017**, *56* (2), 610–614.
- (69) Han, S.; Hu, X.; Wang, J.; Fang, X.; Zhu, Y. Novel Route to Fe-Based Cathode as an Efficient Bifunctional Catalysts for Rechargeable Zn–Air Battery. *Adv. Energy Mater.* **2018**, *8* (22), 1800955.
- (70) Lee, D. U.; Choi, J.-Y.; Feng, K.; Park, H. W.; Chen, Z. Advanced Extremely Durable 3D Bifunctional Air Electrodes for Rechargeable Zinc-Air Batteries. *Adv. Energy Mater.* **2014**, *4* (6), 1301389.
- (71) Cheng, Y.; Dou, S.; Veder, J.-P.; Wang, S.; Saunders, M.; Jiang, S. P. Efficient and Durable Bifunctional Oxygen Catalysts Based on NiFeO@MnO<sub>x</sub> Core–Shell Structures for Rechargeable Zn–Air Batteries. *ACS Appl. Mater. Interfaces* **2017**, *9* (9), 8121–8133.
- (72) Liu, Z.-Q.; Cheng, H.; Li, N.; Ma, T. Y.; Su, Y.-Z. ZnCo<sub>2</sub>O<sub>4</sub> Quantum Dots Anchored on Nitrogen-Doped Carbon Nanotubes as Reversible Oxygen Reduction/Evolution Electrocatalysts. *Adv. Mater.* **2016**, *28* (19), 3777–3784.
- (73) Xia, W.; Mahmood, A.; Liang, Z.; Zou, R.; Guo, S. Earth-Abundant Nanomaterials for Oxygen Reduction. *Angew. Chem. Int. Ed.* **2016**, *55* (8), 2650–2676.

Table of Contents

